Fig S1

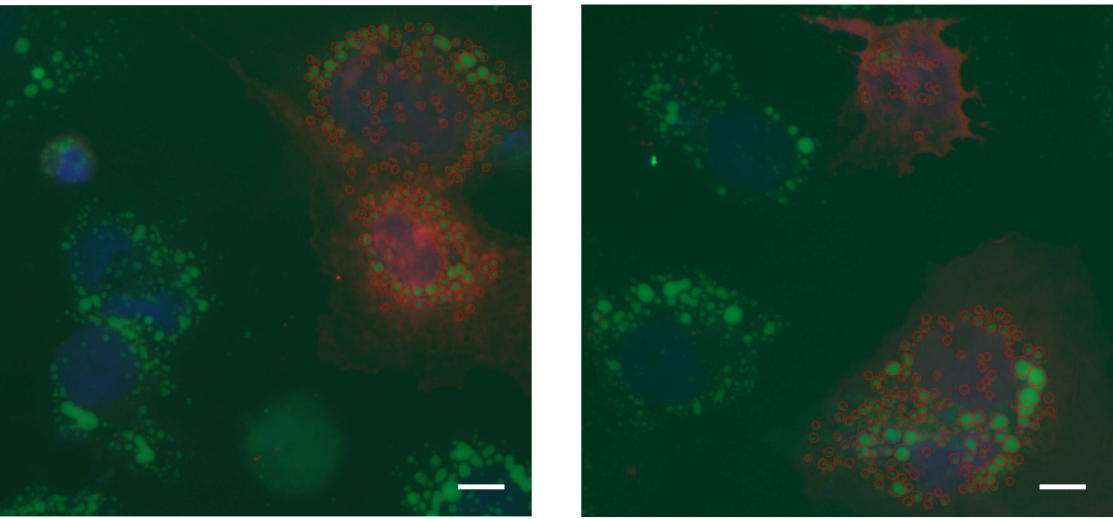

Fig. S1. Quantitation of lipid droplets in oleic acid-treated Huh7 cells. Lipid droplets were stained with BODIPY 493/503 and imaged as described in Materials and Methods. Lipid droplet accumulation was quantitated by drawing a circle around each droplet using the Zeiss Zen 2.3 lite software package to measure the diameter and area; two such images with circled lipid droplets are shown. Scale bar, 10 μm.

Fig S2

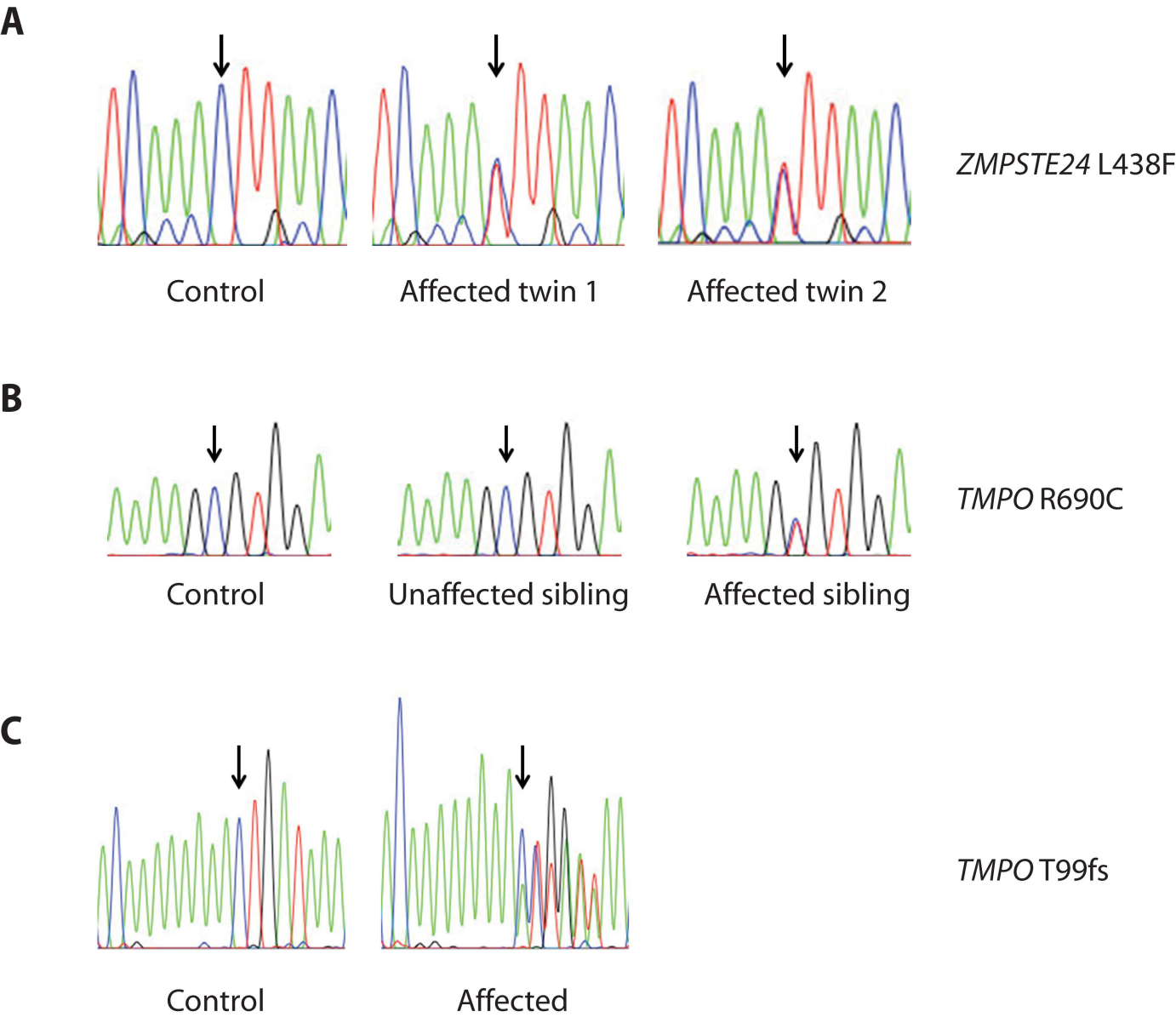

Fig. S2. Selected chromatograms showing confirmation of lamina-related variants in individuals with NAFLD. (A) Two twins with NAFLD carrying the L438F variant in the gene encoding the ZMPSTE24 protease, which cleaves lamin A (C > T change in genomic DNA). (B) NAFLD patient with C > T change in *TMPO* (which encodes the six isoforms of LAP2), resulting in the LAP2α R690C variant. An unrelated control and the patient's unaffected sibling are shown for comparison. (C) NAFLD patient with single base-pair insertion in *TMPO* resulting in a frameshift (fs) and premature stop codon after Thr 99 in the LAP2 protein. Arrows indicate the changed nucleotide in each case; all variants were confirmed by Sanger sequencing of both sense and antisense strands.

Fig S3

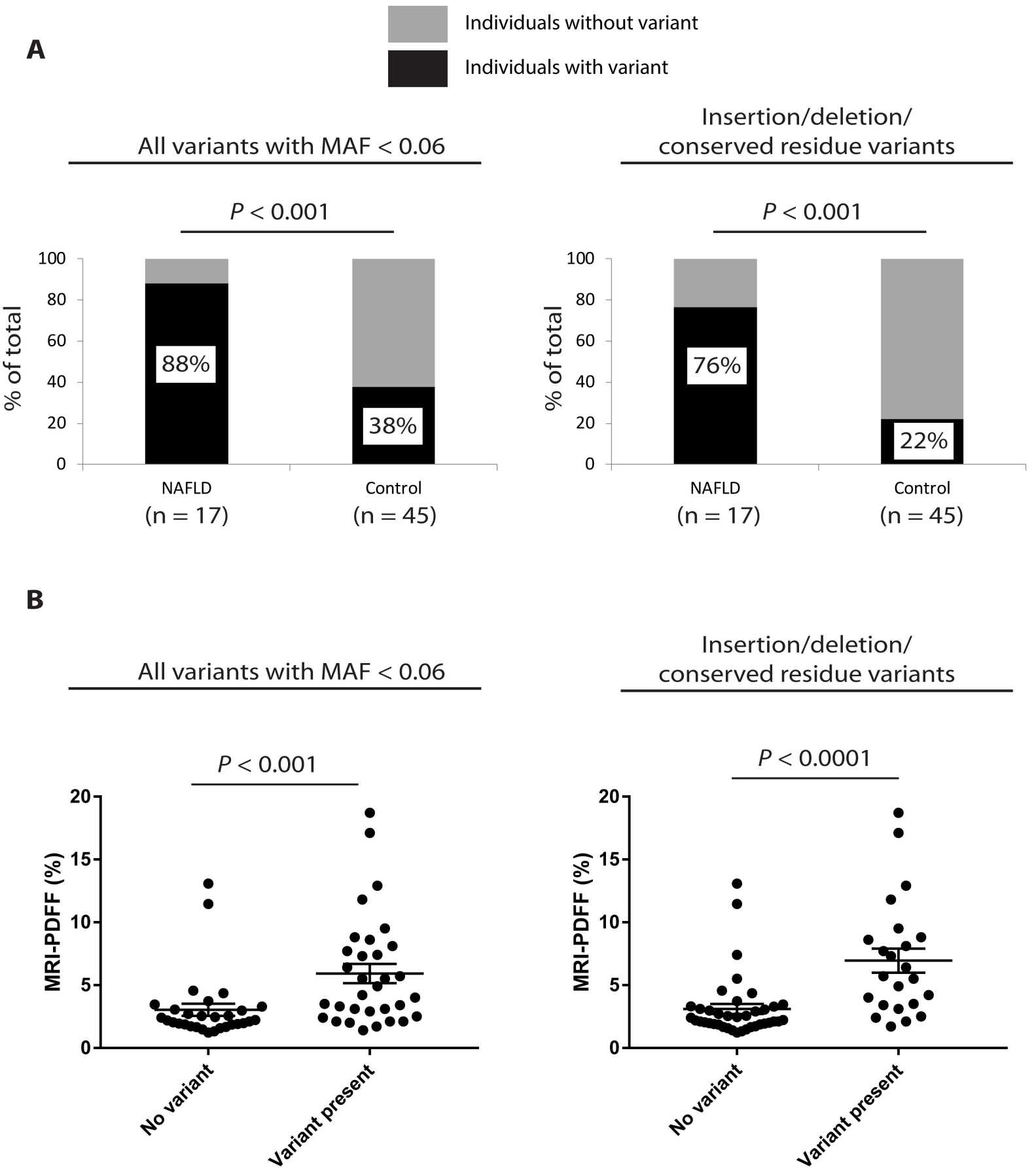
A
Individuals without variant
Individuals with variant
All variants with MAF < 0.06
P < 0.001
% of total
100
80
60
40
20
0
88%
38%
NAFLD
(n = 17)
Control
(n = 45)
Insertion/deletion/
conserved residue variants
P < 0.001
76%
22%
B
All variants with MAF < 0.06
P < 0.001
MRI-PDFF (%)
20
15
10
5
0
No variant
Variant present
Insertion/deletion/
conserved residue variants
P < 0.0001

Fig. S3. Among twin pairs only (31 pairs, n=62 subjects), variants in lamina-related genes were predominantly found in twins with NAFLD. (A) *Left panel*: Percentages of twins (*y*-axis) with and without genetic variants are shown for NAFLD cases and Controls (includes all coding variants with minor allele frequency < 0.06). *Right panel:* Percentages of twins (*y*-axis) with and without a variant resulting in insertion/deletion or change in a conserved residue are shown for NAFLD cases and Controls. Fisher's exact test was used to assess statistical significance at a threshold of $P<0.05$. (B) *Left panel*: Scatter plot of liver fat content (assessed by MRI-PDFF) of twins (31 pairs, n=62 subjects) without and with a lamina-related genetic variant (includes all coding variants with minor allele frequency < 0.06). *Right panel*: Scatter plot of liver fat content (assessed by MRI-PDFF) of twins without and with a lamina-related genetic variant (includes variants resulting in insertion/deletion or change in a conserved residue). Error bars represent standard error of the mean; Mann-Whitney U test was used to assess statistical significance at a threshold of $P<0.05$.

Fig S4

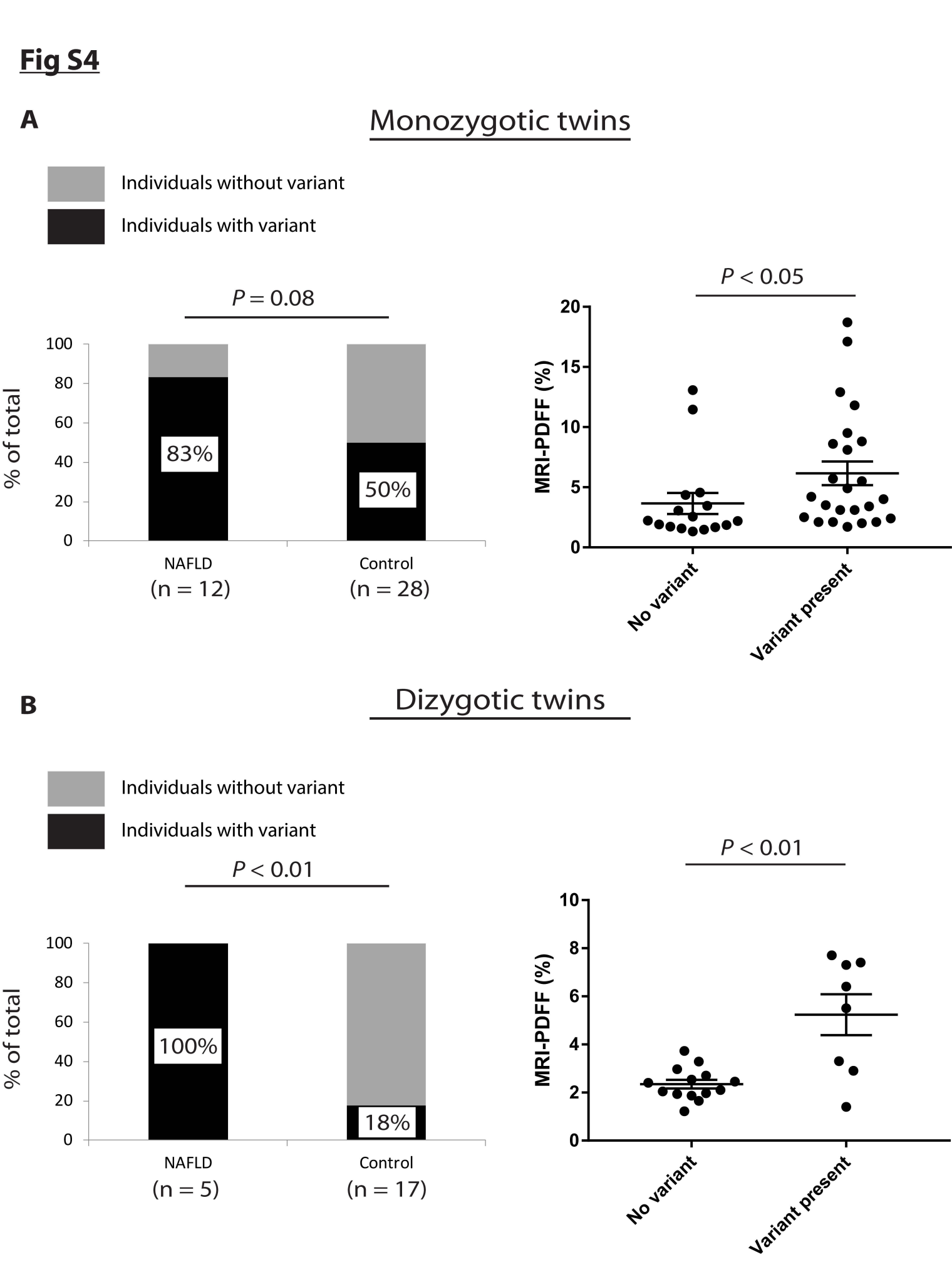
A
Monozygotic twins
Individuals without variant
Individuals with variant
P = 0.08
% of total
100
80
60
40
20
0
83%
50%
NAFLD
(n = 12)
Control
(n = 28)
P < 0.05
MRI-PDFF (%)
20
15
10
5
0
No variant
Variant present
B
Dizygotic twins
Individuals without variant
Individuals with variant
P < 0.01
% of total
100
80
60
40
20
0
100%
18%
NAFLD
(n = 5)
Control
(n = 17)
P < 0.01
MRI-PDFF (%)
10
8
6
4
2
0
No variant
Variant present

Fig. S4. Among both monozygotic (A) and dizygotic twins (B), variants in lamina-related genes were predominantly found in twins with NAFLD. (A) Monozygotic twin pairs (20 pairs, n=40 subjects). *Left panel*: Percentages of monozygotic twins (*y*-axis) with and without genetic variant(s) are shown for both NAFLD cases (n=12) and Controls (n=28) (includes all coding variants with minor allele frequency < 0.06). Fisher's exact test was used to assess statistical significance at a threshold of $P<0.05$. *Right panel:* Scatter plot of liver fat content (assessed by MRI-PDFF) of monozygotic twins without (n=16) and with (n=24) a lamina-related genetic variant (includes all coding variants with minor allele frequency < 0.06). Error bars represent standard error of the mean; Mann-Whitney U test was used to assess statistical significance at a threshold of $P<0.05$. (B) Dizygotic twin pairs (11 pairs, n=22 subjects). *Left panel*: Percentages of twins (*y*-axis) with and without genetic variant(s) are shown for both NAFLD cases (n=5) and Controls (n=17) (includes all coding variants with minor allele frequency < 0.06). Fisher's exact test was used to assess statistical significance at a threshold of $P<0.05$. *Right panel:* Scatter plot of liver fat content (assessed by MRI-PDFF) of twins without (n=14) and with (n=8) a lamina-related genetic variant (includes all coding variants with minor allele frequency < 0.06). Error bars represent standard error of the mean; Mann-Whitney U test was used to assess statistical significance at a threshold of $P<0.05$.

Fig S5

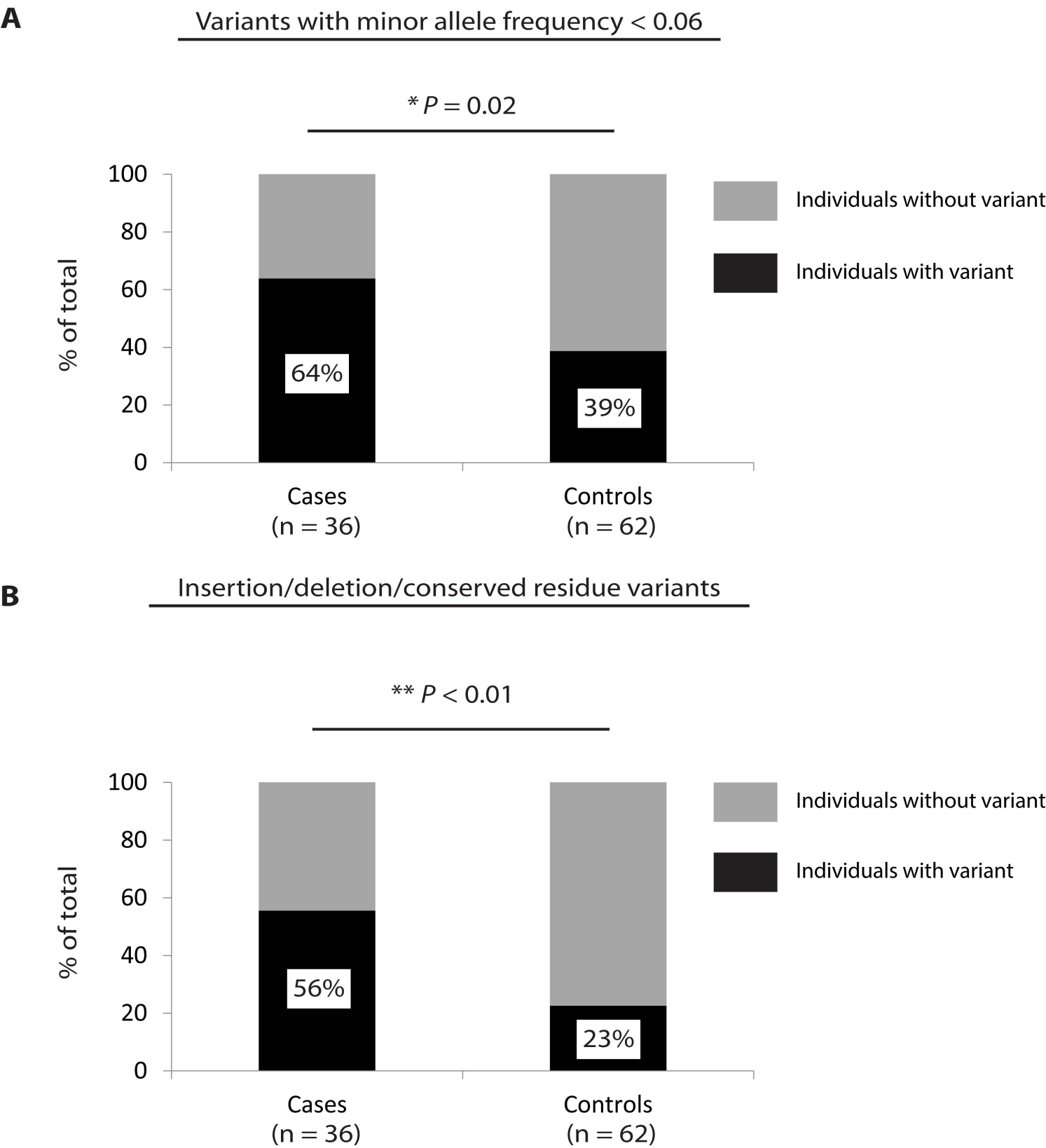
A
Variants with minor allele frequency < 0.06
* P = 0.02
100
80
60
40
20
0
% of total
64%
39%
Cases
(n = 36)
Controls
(n = 62)
Individuals without variant
Individuals with variant
B
Insertion/deletion/conserved residue variants
** P < 0.01
100
80
60
40
20
0
% of total
56%
23%
Cases
(n = 36)
Controls
(n = 62)
Individuals without variant
Individuals with variant

Fig. S5. Among all subjects (n=98), including both twin/sibling pairs (n=74) and additional subjects not part of a twin/sibling pair (n=24), variants in lamina-related genes were predominantly found in individuals with NAFLD. (A) Percentages of individuals (*y*-axis) with and without genetic variant(s) are shown for both NAFLD cases (n=36) and controls (n=62) (includes all coding variants with minor allele frequency < 0.06). (B) Percentages of individuals (*y*-axis) with and without a variant resulting in insertion/deletion or change in a conserved residue are shown for NAFLD cases (n=36) and controls (n=62). Fisher's exact test was used to assess statistical significance at a threshold of $P<0.05$.

Fig S6

A

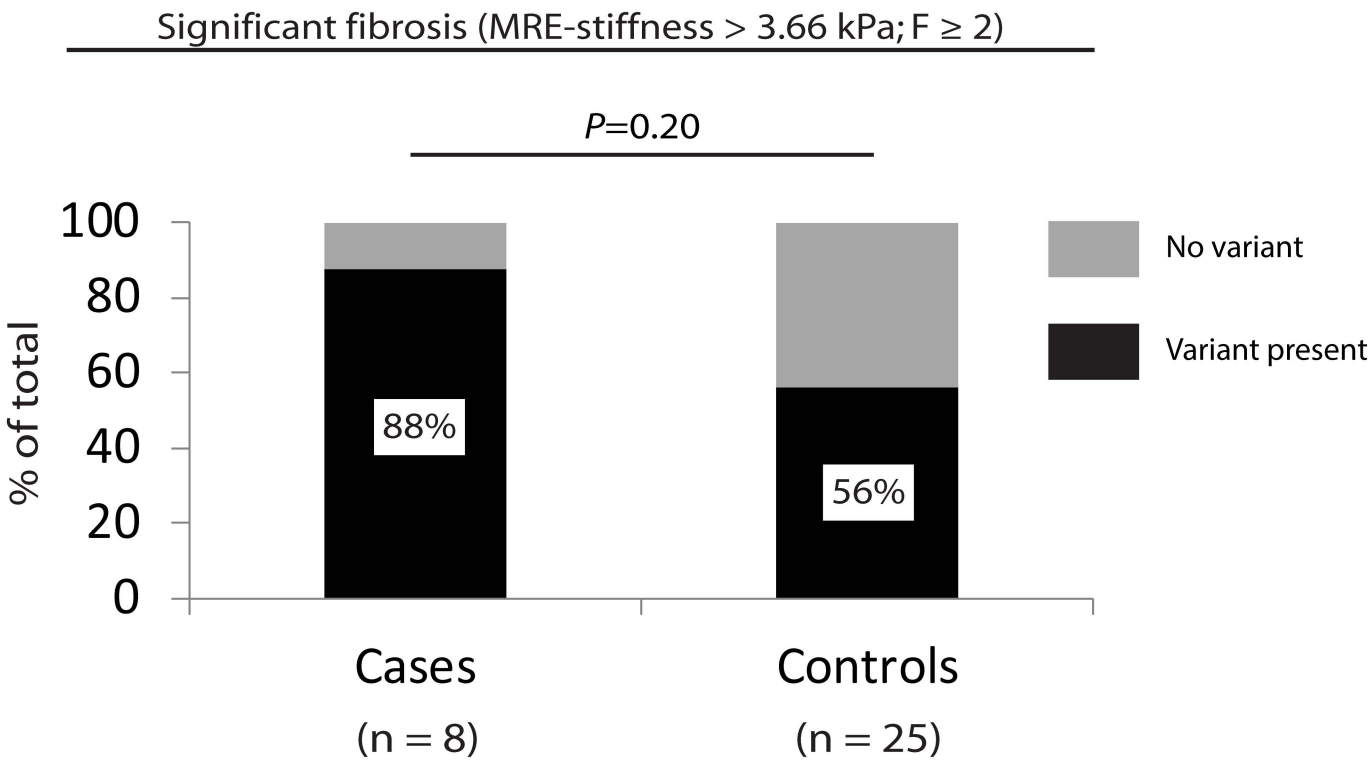
Significant fibrosis (MRE-stiffness > 3.66 kPa; F ≥ 2)
P=0.20
100
80
60
40
20
0
% of total
88%
56%
No variant
Variant present
Cases
(n = 8)
Controls
(n = 25)

B

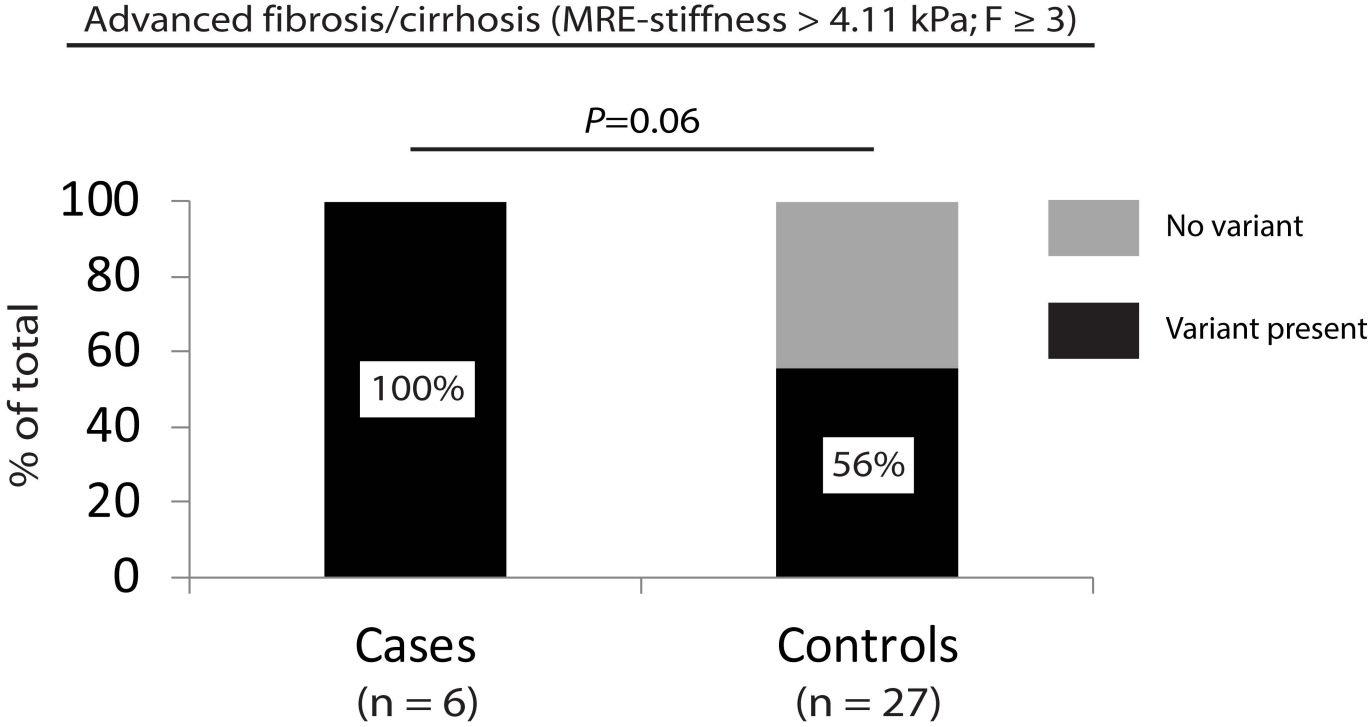
Advanced fibrosis/cirrhosis (MRE-stiffness > 4.11 kPa; F ≥ 3)
P=0.06
100
80
60
40
20
0
% of total
100%
56%
No variant
Variant present
Cases
(n = 6)
Controls
(n = 27)

Fig. S6. Lamina-related variants among study participants with NAFLD and hepatic fibrosis. (A) Significant fibrosis: Percentages of individuals (*y*-axis) with and without genetic variant(s) are shown for both Cases (NAFLD with MRE > 3.66 kPa; F ≥ 2) and Controls (NAFLD with MRE < 3.66 kPa; F < 2). (B) Advanced fibrosis/cirrhosis: Percentages of individuals (*y*-axis) with and without genetic variant(s) are shown for both cases (NAFLD with MRE > 4.11 kPa; F ≥ 3) and controls (NAFLD with MRE < 4.11 kPa; F < 3). For each group, Fisher's exact test was used to assess statistical significance at a threshold of $P<0.05$. Note that this analysis includes twins and siblings with NAFLD (n=20 twins/siblings with NAFLD and MRE data) as well as additional subjects with NAFLD who were not part of a twin/sibling pair (n=13 subjects with NAFLD and MRE data); n=33 total subjects.

Fig S7

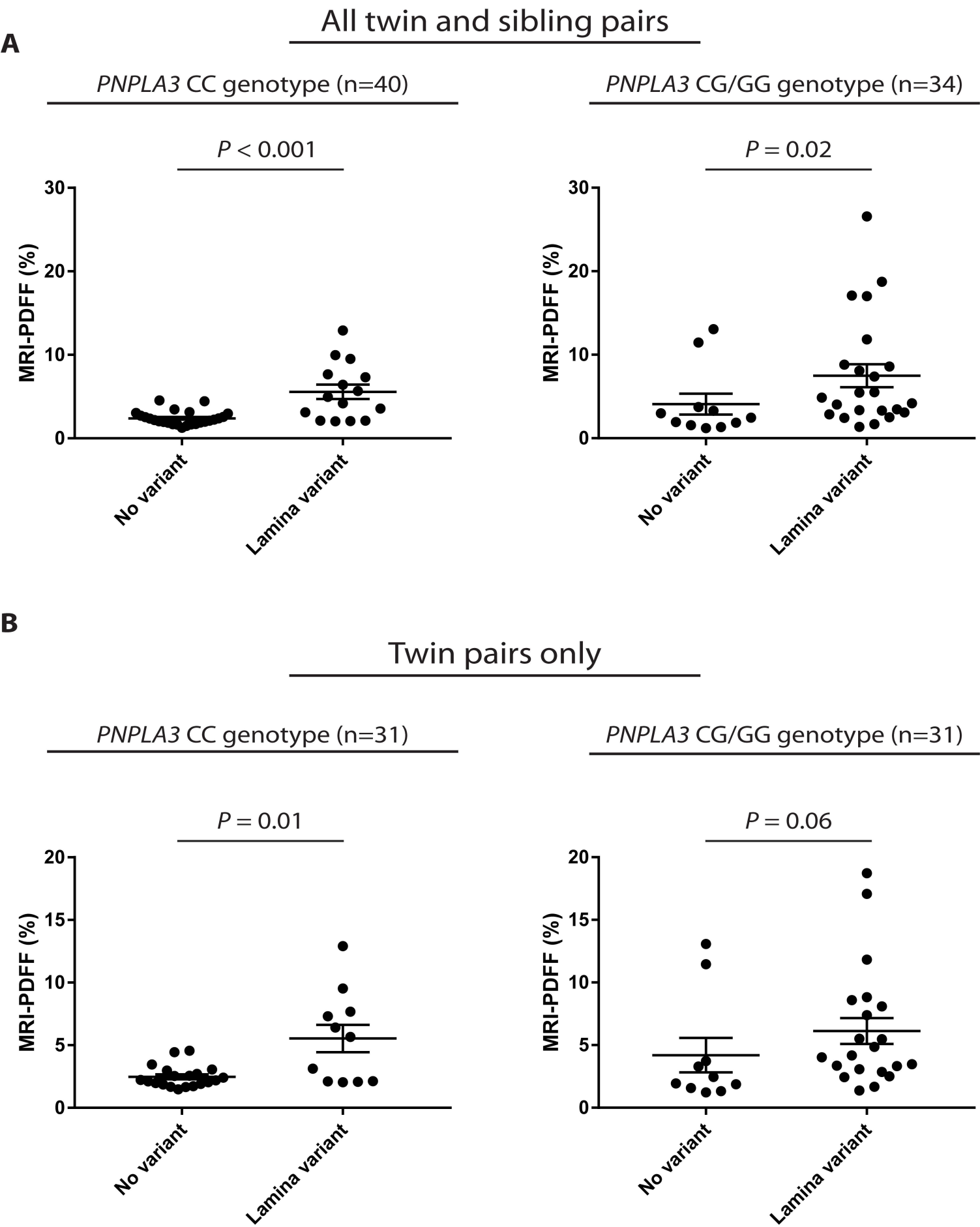
A
All twin and sibling pairs
PNPLA3 CC genotype (n=40)
P < 0.001
MRI-PDFF (%)
30
20
10
0
No variant
Lamina variant
PNPLA3 CG/GG genotype (n=34)
P = 0.02
MRI-PDFF (%)
30
20
10
0
No variant
Lamina variant
B
Twin pairs only
PNPLA3 CC genotype (n=31)
P = 0.01
MRI-PDFF (%)
20
15
10
5
0
No variant
Lamina variant
PNPLA3 CG/GG genotype (n=31)
P = 0.06
MRI-PDFF (%)
20
15
10
5
0
No variant
Lamina variant

Fig. S7. Presence or absence of lamina-related genetic variants stratified by *PNPLA3* genotype. (A) All twin and sibling pairs (37 pairs, n=74 subjects). *Left panel*: Scatter plot of liver fat content (assessed by MRI-PDFF) of the 40 subjects with *PNPLA3* CC genotype without and with a lamina-related genetic variant. *Right panel*: Scatter plot of liver fat content (assessed by MRI-PDFF) of the 34 subjects with *PNPLA3* CG or GG genotype without and with a lamina-related genetic variant. Error bars represent standard error of the mean; Mann-Whitney U test was used to assess statistical significance at a threshold of $P<0.05$. (B) Twin pairs only (31 pairs, n=62 subjects). *Left panel*: Scatter plot of liver fat content (assessed by MRI-PDFF) of the 31 twins with *PNPLA3* CC genotype without and with a lamina-related genetic variant. *Right panel*: Scatter plot of liver fat content (assessed by MRI-PDFF) of the 31 twins with *PNPLA3* CG or GG genotype without and with a lamina-related genetic variant. Error bars represent standard error of the mean; Mann-Whitney U test was used to assess statistical significance at a threshold of $P<0.05$. Note that subjects with *PNPLA3* CG and GG genotypes were grouped for these analyses due to the small number of GG homozygotes (n=12) in the cohort.

Fig S8

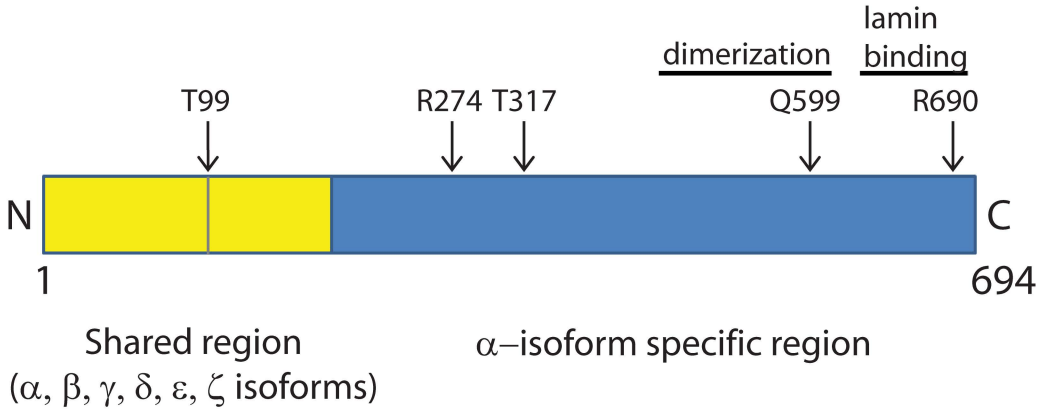

Fig. S8. Schematic of the LAP2α protein. The *TMPO* gene encodes six isoforms of LAP2, which are derived via alternative splicing. As shown, four of the five genetic variants in *TMPO* identified in this study were in the portion of the gene unique to the α isoform (blue shading), which is known to interact with lamin A. The fifth variant (within the yellow shading) was a single basepair insertion causing a frameshift and premature stop codon after Thr 99 in the translated protein.

Fig S9

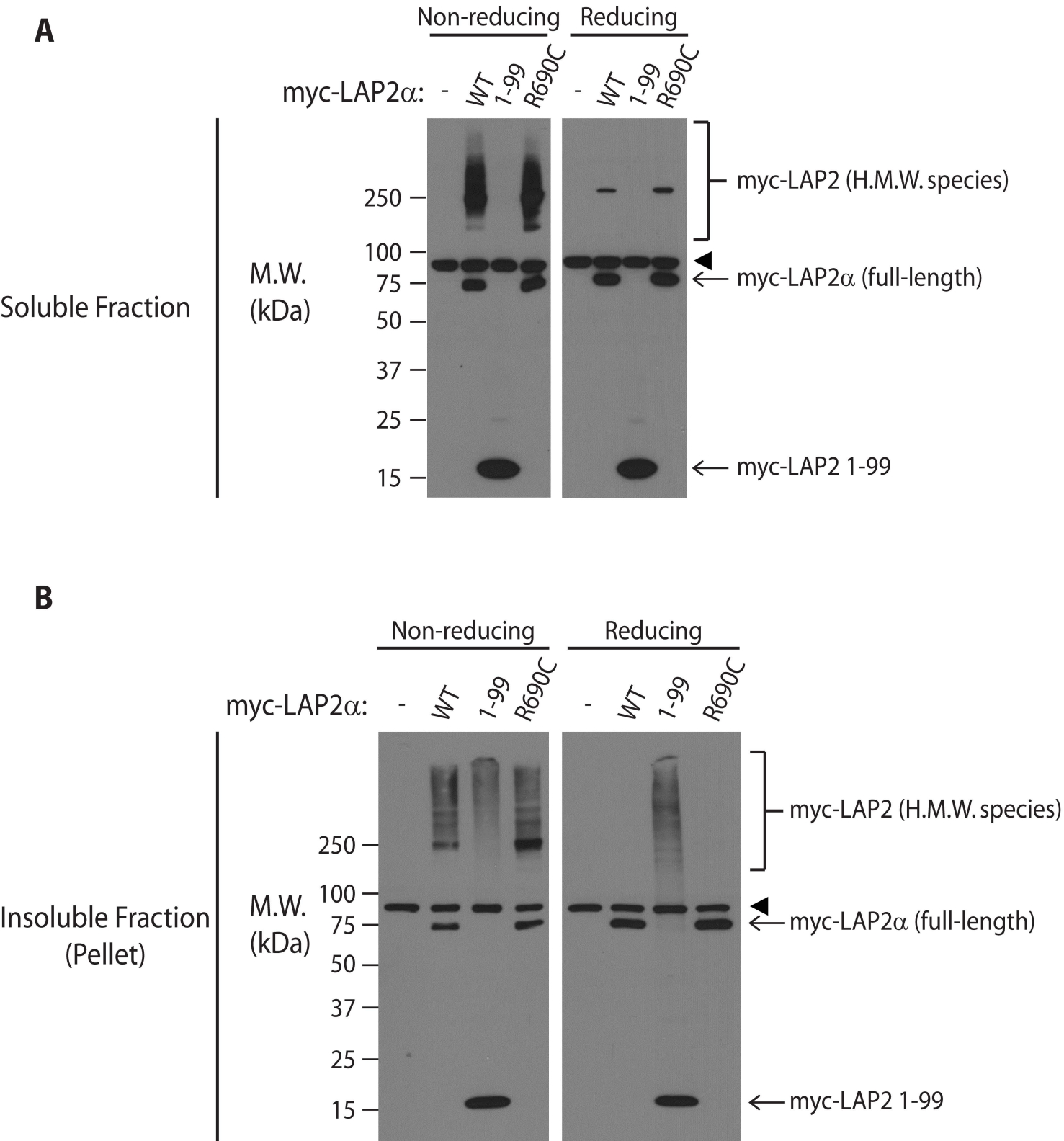
A
Non-reducing
Reducing
myc-LAP2α:
-
WT
1-99
R690C
-
WT
1-99
R690C
Soluble Fraction
M.W.
(kDa)
250
100
75
50
37
25
15
myc-LAP2 (H.M.W. species)
myc-LAP2α (full-length)
myc-LAP2 1-99
B
Non-reducing
Reducing
myc-LAP2α:
-
WT
1-99
R690C
-
WT
1-99
R690C
Insoluble Fraction
(Pellet)
M.W.
(kDa)
250
100
75
50
37
25
15
myc-LAP2 (H.M.W. species)
myc-LAP2α (full-length)
myc-LAP2 1-99

Fig. S9. Full-length, but not truncated, LAP2α forms a soluble high-molecular weight species under non-reducing conditions. (A) Huh7 cells were transfected with wild-type (WT) LAP2α or the indicated variant. Two days after transfection, cells were harvested and the Triton-soluble fraction was resolved on denaturing SDS-PAGE under non-reducing or reducing conditions. Transfected LAP2 was visualized by immunoblotting with antibody directed to the myc tag. (B) The Triton-insoluble (pellet) fraction of Huh7 cells, transfected as in panel A, was resolved using denaturing SDS-PAGE (non-reducing and reducing) and analyzed by immunoblotting. H.M.W., high molecular weight; M.W., apparent molecular weight; kDa, kilodaltons. Arrowhead highlights a non-specific band recognized by the myc antibody.

Fig S10

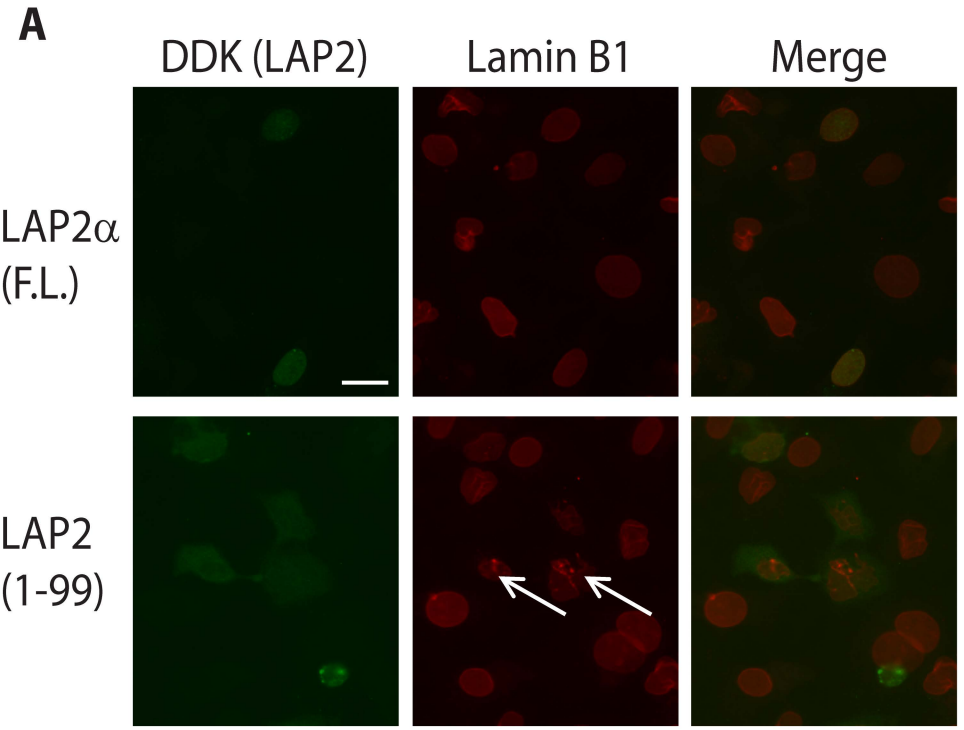
A
DDK (LAP2)
Lamin B1
Merge
LAP2α (F.L.)
LAP2 (1-99)

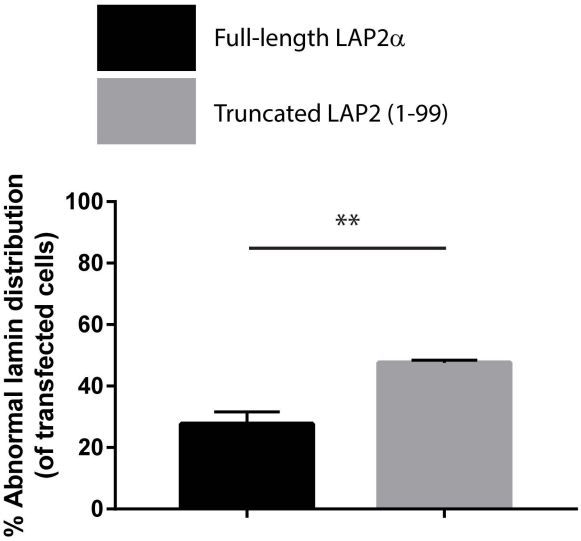
Full-length LAP2α
Truncated LAP2 (1-99)
% Abnormal lamin distribution (of transfected cells)
100
80
60
40
20
0
**

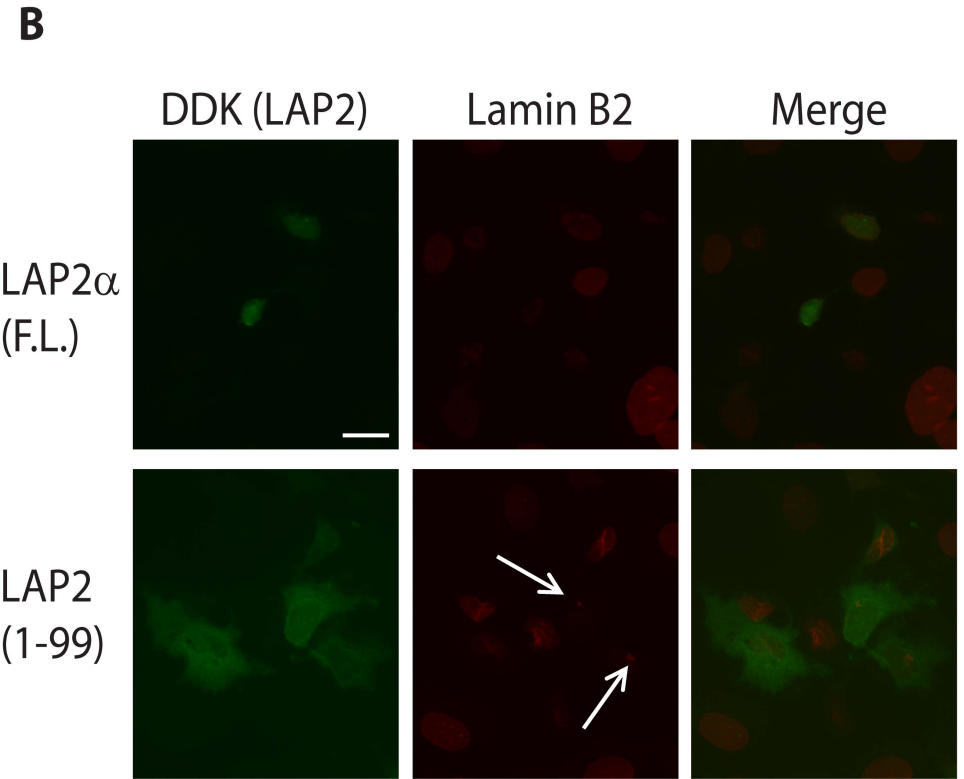
B
DDK (LAP2)
Lamin B2
Merge
LAP2α (F.L.)
LAP2 (1-99)

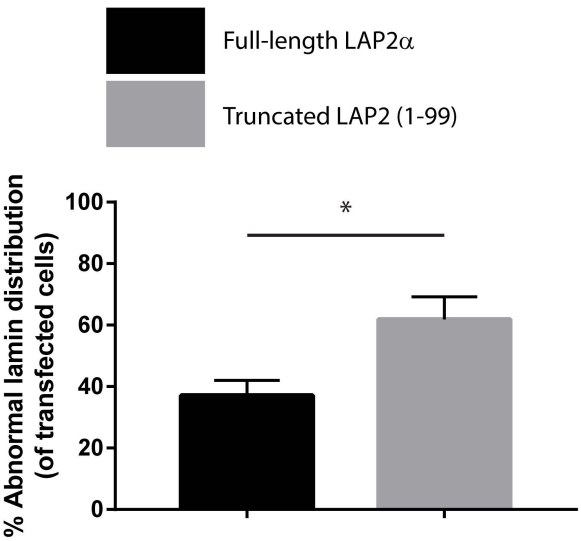
Full-length LAP2α
Truncated LAP2 (1-99)
% Abnormal lamin distribution (of transfected cells)
100
80
60
40
20
0
*

Fig. S10. Truncated LAP2 alters B-type lamin distribution. (A) Huh7 cells were transfected with DDK-tagged full-length (F.L.) LAP2α or truncated LAP2 (1-99). After fixation, transfected LAP2 and endogenous lamin B1 were visualized by immunofluorescence using anti-FLAG and anti-lamin B1 antibodies, respectively. Representative high-magnification images are shown; nuclei of transfected cells with abnormal lamin staining (punctate/globular) are indicated by arrows. Scale bar, 20 μm. Right panel shows quantitation (>40 nuclei scored for each condition). Error bars represent standard error of the mean. Student's *t* test was used to determine statistical significance; **, $P<0.01$. (B) Cells were transfected with full-length or truncated LAP2α with DDK tag as in panel A. After fixation, transfected LAP2 and endogenous lamin B2 were visualized by immunofluorescence using anti-FLAG and anti-lamin B2 antibodies, respectively. Representative high-magnification images are shown; nuclei of transfected cells with abnormal lamin staining (punctate/globular) are indicated by arrows. Scale bar, 20 μm. Right panel shows quantitation (>40 nuclei scored for each condition). Error bars represent standard error of the mean. Student's *t* test was used to determine statistical significance; *, $P<0.05$.

Primer Name	Variant	Sequence (5' → 3')
ZMPSTE24-L438F-FWD	*ZMPSTE24* L438F	TTTCTGGCCTGTTTGCTTGG
ZMPSTE24-L438F-REV	*ZMPSTE24* L438F	CATGCTGCCAGGACAGAAAT
BANF1-G21E-FWD	*BANF1* G21E	GGGAAGAGTCTCCCTGGAAC
BANF1-G21E-REV	*BANF1* G21E	TGCCATTCAGAGCACACAAG
TMPO-T99fs-FWD	*TMPO* T99fs	AGTTACTTGCTTGGCTGTGC
TMPO-T99fs-REV	*TMPO* T99fs	GTCCTTGGAACCTAAACTGCT
TMPO-R274K-FWD	*TMPO* R274K; *TMPO* T317S	TCTTGTTGCCACAAACTTGC
TMPO-R274K-REV	*TMPO* R274K; *TMPO* T317S	CCAGTGGGGGCATAGAGTTA
TMPO-Q599E-FWD	*TMPO* Q599E	TGGCATGCAAATATCCAGTTTC
TMPO-Q599E-REV	*TMPO* Q599E	AATCCTTCAGCCAGAGGTATCG
TMPO-R690C-FWD	*TMPO* R690C	CGCTTGGGATTCTGAGCAAA
TMPO-R690C-REV	*TMPO* R690C	ATTGTTTGTACCAGGCTTCCT
SREBF1-V610M-FWD	*SREBF1* V610M	GGGACAGATTCATGGTGTGCACAGG
SREBF1-V610M-REV	*SREBF1* V610M	GAACTTGGGGCTCTGGATTTCCTGG
SREBF2-S72ins-FWD	*SREBF2* S72ins	GAAAGAGGTAAGGGTTTCCTGACCC
SREBF2-S72ins-REV	*SREBF2* S72ins	CTTGACTTGCAGAGTTGGAGCCTGTG
SREBF2-R371K-FWD	*SREBF2* R371K	TAACTTCTCCCGAGTGGCAC
SREBF2-R371K-REV	*SREBF2* R371K	CCACCTCATTGTCCACCAGA
SREBF2-G595A-FWD	*SREBF2* G595A	GGAAATACCTCAGAATGTCAGCAGGG
SREBF2-G595A-REV	*SREBF2* G595A	GCTGGTCTTAGCTTCGTCTTCAAAGC
SREBF2-R860S-FWD	*SREBF2* R860S	GGTCTTAGAGCTGGAGAGCTGAACAG
SREBF2-R860S-REV	*SREBF2* R860S	GAACTGGAGCCACAGGTATGAACCTG
SREBF2-R1080Q-FWD	*SREBF2* R1080Q	CTTTTCCGTGGATTGGGTGG
SREBF2-R1080Q-REV	*SREBF2* R1080Q	CCACTCTCAGCGGGAAGAT

Table S1. Primers used for PCR amplification of genomic DNA and Sanger sequencing.

Antibody target	Manufacturer	Catalog/clone number	Dilution
FLAG / DDK tag	Sigma-Aldrich	F1804 (clone M2)	1:250 (IF)
GFP	Origene	TA150041 (clone 2H8)	1:2000 (IB); 1.5 µg per 500 µL lysate (IP)
Myc tag	Abcam	ab9106	1:1000 (IB)
Lamin A/C	Santa Cruz Biotechnology	sc-20681 (H-110)	1:250 (IF)
Lamin B1	Abcam	ab16048	1:250 (IF)
Lamin B2	Cell Signaling	12255 (clone D8P3U)	1:250 (IF)
p62/SQSTM1	Abcam	ab96706	1:2000 (IB)

Table S2. Antibodies used for immunofluorescence (IF), immunoprecipitation (IP), and immunoblotting (IB).

Gene	Protein	Associated disease(s)
LMNA	A-type lamin	Dilated cardiomyopathy, progeria, lipodystrophy, Charcot-Marie-Tooth disease, muscular dystrophy (1-9)
LMNB2	B-type lamin	Lipodystrophy (10)
ZMPSTE24	Lamin-processing enzyme	Mandibuloacral dysplasia, lipodystrophy, restrictive dermopathy (11, 12)
ICMT	Lamin-processing enzyme	None known
FNTA	Lamin-processing enzyme	None known
FNTB	Lamin-processing enzyme	None known
TMPO	Lamin binding partner	Dilated cardiomyopathy (13)
BANF1	Lamin binding partner	Atypical progeria (14)
SREBF1	Transcription factor	None known
SREBF2	Transcription factor	None known

Table S3. Candidate genes sequenced.

Table S4. LAP2 interacting proteins as determined by mass spectrometry (appended separately).

TWIN ID	Sex	Age (yrs)	NAFLD	Diabetes	Other chronic disease	*PNPLA3* genotype	Height (m)	Weight (kg)	BMI (kg/ m^2)	Alcohol use	ALT (IU/L)	Glucose (mg/dL)	Insulin (µU/mL)	HOMA-IR	TG (mg/dL)
TW01	M	41	No	No	No	CG	1.73	83.9	28	None	26	92	8	1.8	79
TW02	M	41	Yes	No	No	CG	1.74	100.6	33	Rare (less than once per week)	26	90	14	3.1	172

Table S5. Clinical and laboratory data for monozygotic twins TW01 and TW02 carrying insertion in *TMPO*. U, units; IU, international units; HOMA-IR, homeostatic model of insulin resistance; TG, triglycerides.

Supplementary Methods

Study participant recruitment and clinical data acquisition. All participants (recruited between January 2012 and January 2015) underwent a standardized clinical research visit at the University of California San Diego (UCSD) NAFLD Translational Research Unit including detailed medical history, assessment of alcohol consumption, physical examination, testing to exclude other causes of chronic liver disease, fasting laboratory tests (see below), and magnetic resonance imaging (MRI) examination of the liver. Research visits and MRI procedures for each related pair were performed on the same day. The Alcohol Use Disorders Identification Test questionnaire and Skinner Lifetime Drinking history were administered to record and quantify alcohol use. A physical examination including vital signs, height, weight, and anthropometric measurements was performed. Body mass index (BMI) was calculated by dividing body weight by the square of the height (kilogram/meters^2). Fasting laboratory studies were obtained for all participants including complete blood count, liver disease screening tests (hepatitis B surface antigen, hepatitis C antibody, and iron panel including serum ferritin), clinical chemistry (creatinine, total protein, blood urea nitrogen, uric acid), hemoglobin A1c, hepatic panel (total bilirubin, direct bilirubin, aspartate aminotransferase, alanine aminotransferase [ALT], alkaline phosphatase, γ-glutamyltransferase, albumin, prothrombin time, and international normalized ratio), lipid profile, and glucose/insulin levels. MRI examinations were performed using a 3T research scanner (GE Signa EXCITE HDxt; GE Healthcare, Waukesha, WI) at the UCSD MR3T Research Laboratory. Liver fat was measured via MRI-determined proton-density fat-fraction (MRI-PDFF), and liver fibrosis was quantified by MR elastography-determined stiffness (MRE-stiffness) as described (15). NAFLD was defined as MRI-PDFF ≥5%

without apparent secondary cause of hepatic steatosis such as significant alcohol use, use of steatogenic medication(s), or other cause of liver disease.

Next-generation DNA sequencing and variant identification: Next-generation sequence data was obtained from genomic DNA by amplification of target regions with a custom Illumina TruSeq amplicon panel and analysis via Illumina MiSeq instrument. Sequences were then trimmed using Trimmomatic v0.32 and aligned to human reference genome build Grc37/hg19 using the Burrows-Wheeler Aligner 'mem' algorithm v0.7.8. Variants were detected using the Broad Institute Genome Analysis Toolkit v.3.3-0 Haplotype Caller with default parameters, -strand_emit_conf 10 and -strand_call_conf 30, DISCOVERY mode. Variant filtering, annotation and reporting were performed using VarSeq v.1.1.0 (Golden Helix, Bozeman, MT). Variants with fewer than 5 alternate observations were removed. Variants were annotated based on RefSeq v.69 gene models, and matched with 1000 Genomes Phase 3 population frequency data and dbNSFP v2.0 functional annotations (16, 17).

Supplementary References

1. Worman HJ, Fong LG, Muchir A, Young SG. Laminopathies and the long strange trip from basic cell biology to therapy. J Clin Invest 2009;119:1825-1836.

2. Davidson PM, Lammerding J. Broken nuclei--lamins, nuclear mechanics, and disease. Trends Cell Biol 2014;24:247-256.

3. Hatch E, Hetzer M. Breaching the nuclear envelope in development and disease. J Cell Biol 2014;205:133-141.

4. Taylor MR, Fain PR, Sinagra G, Robinson ML, Robertson AD, Carniel E, Di Lenarda A, et al. Natural history of dilated cardiomyopathy due to lamin A/C gene mutations. J Am Coll Cardiol 2003;41:771-780.

5. **Van Esch H, Agarwal AK**, Debeer P, Fryns JP, Garg A. A homozygous mutation in the lamin A/C gene associated with a novel syndrome of arthropathy, tendinous calcinosis, and progeroid features. J Clin Endocrinol Metab 2006;91:517-521.

6. Guenantin AC, Briand N, Bidault G, Afonso P, Bereziat V, Vatier C, Lascols O, et al. Nuclear envelope-related lipodystrophies. Semin Cell Dev Biol 2014;29:148-157.

7. Bonne G, Di Barletta MR, Varnous S, Becane HM, Hammouda EH, Merlini L, Muntoni F, et al. Mutations in the gene encoding lamin A/C cause autosomal dominant Emery-Dreifuss muscular dystrophy. Nat Genet 1999;21:285-288.

8. Fatkin D, MacRae C, Sasaki T, Wolff MR, Porcu M, Frenneaux M, Atherton J, et al. Missense mutations in the rod domain of the lamin A/C gene as causes of dilated cardiomyopathy and conduction-system disease. N Engl J Med 1999;341:1715-1724.

9. Ajluni N, Meral R, Neidert AH, Brady GF, Buras E, McKenna B, DiPaola F, et al. Spectrum of disease associated with partial lipodystrophy: lessons from a trial cohort. Clin Endocrinol (Oxf) 2017;86:698-707.

10. Hegele RA, Cao H, Liu DM, Costain GA, Charlton-Menys V, Rodger NW, Durrington PN. Sequencing of the reannotated LMNB2 gene reveals novel mutations in patients with acquired partial lipodystrophy. Am J Hum Genet 2006;79:383-389.

11. Agarwal AK, Fryns JP, Auchus RJ, Garg A. Zinc metalloproteinase, ZMPSTE24, is mutated in mandibuloacral dysplasia. Hum Mol Genet 2003;12:1995-2001.

12. Navarro CL, De Sandre-Giovannoli A, Bernard R, Boccaccio I, Boyer A, Genevieve D, Hadj-Rabia S, et al. Lamin A and ZMPSTE24 (FACE-1) defects cause nuclear disorganization and identify restrictive dermopathy as a lethal neonatal laminopathy. Hum Mol Genet 2004;13:2493-2503.

13. Taylor MR, Slavov D, Gajewski A, Vlcek S, Ku L, Fain PR, Carniel E, et al. Thymopoietin (lamina-associated polypeptide 2) gene mutation associated with dilated cardiomyopathy. Hum Mutat 2005;26:566-574.

14. Puente XS, Quesada V, Osorio FG, Cabanillas R, Cadinanos J, Fraile JM, Ordonez GR, et al. Exome sequencing and functional analysis identifies BANF1 mutation as the cause of a hereditary progeroid syndrome. Am J Hum Genet 2011;88:650-656.

15. Loomba R, Schork N, Chen CH, Bettencourt R, Bhatt A, Ang B, Nguyen P, et al. Heritability of Hepatic Fibrosis and Steatosis Based on a Prospective Twin Study. Gastroenterology 2015;149:1784-1793.

16. 1000 Genomes Project Consortium (Auton A, Brooks LD, Durbin RM, Garrison EP, Kang HM, Korbel JO, et al.). A global reference for human genetic variation. Nature 2015;526:68-74.

17. Liu X, Jian X, Boerwinkle E. dbNSFP v2.0: a database of human non-synonymous SNVs and their functional predictions and annotations. Hum Mutat 2013;34:E2393-2402.